Article

Regulatory Mechanism of Iron, Potassium, and Manganese on the Mycelial Growth of *Lentinula edodes* Revealed by Transcriptome Analysis

Shengle Zhou [†] , Runze Huang [†] , Xianao Pan , Honglei Wang [*]

Posted Date: 21 April 2026

doi: 10.20944/preprints202604.1406.v1

Keywords: *Lentinula edodes*; metal ions; mycelial growth; transcriptome; differentially expressed genes

 doi:10.20944/preprints202604.1406.v1

Article

Regulatory Mechanism of Iron, Potassium, and Manganese on the Mycelial Growth of *Lentinula edodes* Revealed by Transcriptome Analysis

Shengle Zhou [1,†], Runze Huang [1,†], Xianao Pan [1] and HongLei Wang [1,2,*]

[1] Yantai Institute of China Agricultural University, Yantai 264670, China

[2] Yantai Edible and Medicinal Mushroom Technology Innovation Center, Yantai 264670, China

* Correspondence: whl197749@163.com or wanghonglei@cau.edu.cn; Tel.: +86-13287988606

[†] These authors contributed equally to this work.

Abstract

Lentinula edodes (*L. edodes*) is a significant edible and medicinal mushroom with essential nutrient elements for its growth, including Fe^{2+}, K^+, and Mn^{2+}. However, the molecular mechanisms by which these metal ions regulate the mycelial growth of *L. edodes* have been poorly elucidated at the transcriptomic level. In this study, plate culture was performed using concentration gradients to screen for optimal concentrations. Transcriptome sequencing (RNA-seq) and qRT-PCR validation were performed to elucidate the regulatory effects and molecular mechanisms of the three metal ions on the mycelial growth of *L. edodes*. The results showed that Fe^{2+} at concentrations above 20 μg/mL significantly inhibited mycelial growth; K^+ at 1200 μg/mL and Mn^{2+} at 50 μg/mL significantly promoted mycelial growth, with increases of 21.22% and 10.77%, respectively. Transcriptomic analysis revealed that Fe^{2+} primarily induced abnormal protein folding and suppressed material and energy metabolism, thus inhibiting mycelial growth. Mycelial growth is promoted by K^+ by enhancing detoxification and secondary metabolism and by activating mitochondrial function and the oxidative phosphorylation pathway. The proliferation and growth of mycelial cells are regulated by Mn^{2+} through mechanisms that govern DNA repair and recombination, cell cycle progression, and detoxification. This study elucidates the differential regulatory mechanisms of the three metal ions on the mycelial growth of *L. edodes* at the transcriptomic level, offering a rationale for enhancing mineral nutrition and high-yield cultivation of *L. edodes*.

Keywords: *Lentinula edodes*; metal ions; mycelial growth; transcriptome; differentially expressed genes

1. Introduction

Lentinula edodes (*L. edodes*) is a prominent edible fungus in the phylum Basidiomycota with thick, fleshy fruiting bodies that have a unique flavor and are rich in various bioactive components, including polysaccharides, proteins, minerals, and ergosterol[1–3]. Nearly all the essential amino acids that are essential to humans are encoded in this fungus[4]. It offers both nutritional and medicinal benefits with multiple biological effects, including anti-tumor activity, regulation of cardiovascular functions, and immune system enhancement[1,5,6], and is cultivated widely across the globe[2].

Edible fungi possess a high capacity for absorbing metal ions from the culture medium due to their ability to bioaccumulate metal ions and convert them into bioavailable forms from the culture medium via mycelia[3,7,8]. Research indicates that edible fungi bioaccumulate essential elements from the culture medium into their edible tissues and that their size, shape, texture, or color, yield

 doi:10.20944/preprints202604.1406.v1

loss, fruiting body damage, or a reduction in biological efficiency are not altered by growth in the medium with appropriate element concentrations[9–11]. Studies have confirmed significant regulatory effects of common metal ions such as Fe^{2+}[8,12], Mn^{2+}[13–15], Mg^{2+}[16,17], and Zn^{2+}[9,10,17] on the mycelia, fruiting bodies, and nutritional components of edible fungi, including *Pleurotus ostreatus*, *Antrodia cinnamomea*, *Ganoderma lucidum,* and *Pleurotus eryngii*, and an obvious concentration-dependent pattern is observed in the effects of most metal ions.

The response mechanisms of edible fungi to environmental factors and exogenous nutrients have been widely elucidated by transcriptomic technology[18–22]. However, transcriptomic studies on the regulation of *L. edodes* mycelial growth by metal ions remain insufficient, and the key regulatory genes and core metabolic pathways governing mycelial growth in *L. edodes* under diverse metal ions have not been precisely identified[2]. Based on this, this study systematically established concentration-gradient treatments for three metal ions (Fe^{2+}, K^{+}, and Mn^{2+}) and determined the optimal concentrations of each ion for regulating *L. edodes* mycelial growth through plate culture experiments. Moreover, RNA sequencing (RNA-seq) was performed, and, together with differential expression and functional enrichment analyses, the molecular mechanisms by which different metal ions regulate *L. edodes* mycelial growth were interpreted at the transcriptomic level to identify key regulatory genes and core metabolic pathways. This study aims to advance the molecular theory of metal ion-regulated growth and development in edible fungi and to lay a scientific foundation for optimizing mineral nutrient levels in the culture medium and for developing high-yield, high-quality cultivation techniques for *L. edodes*.

2. Materials and Methods

2.1. Materials

2.1.1. Strain

Lentinula edodes 1303: Preserved in the Laboratory of Microbiology and Food, Yantai Institute of China Agricultural University.

2.1.2. Main Reagents

Potato Dextrose Agar (PDA) medium: Hangzhou Microbial Reagent Co., Ltd.; Potato Dextrose Broth (PDB) medium: Shanghai Boshui Biotechnology Co., Ltd.; $FeSO_4{\cdot}7H_2O$: Tianjin Beichen Fangzheng Reagent Factory; $MnSO_4{\cdot}H_2O$: Shanghai Aladdin Biochemical Technology Co., Ltd.; K_2SO_4: Tianjin Yongda Chemical Reagent Co., Ltd.

2.1.3. Reference Genome

Downloaded from the NCBI database (https://www.ncbi.nlm.nih.gov/datasets/genome/GCF_021015755.1/).

2.2. Methods

2.2.1. Plate Culture Assay

The strain was activated by incubation at 24 °C for 7 days after inoculating on PDA medium. PDA media were prepared with concentration gradients of Fe^{2+} (0, 10, 20, 30, 40 μg/mL), K^{+} (0, 400, 800, 1200, 1600, 2000 μg/mL), and Mn^{2+} (0, 50, 100, 150, 200, 250 μg/mL), respectively. Conventional plate inoculation of *L. edodes* was performed after autoclaving at 121 °C for 20 minutes[23]. It was added to the medium via a bacterial filter after high-temperature sterilization to prevent oxidation of Fe^{2+}[6].

On day 3 of incubation, the colony diameter was measured via the cross method[24], and the growth radius was calculated accordingly. All plate culture assays were performed with six replicates. The data were stated as *mean ± standard error (SE)*. The significant differences among experimental data were analyzed using Duncan's multiple range test in SPSS 26, with a p-value < 0.05

 doi:10.20944/preprints202604.1406.v1

considered statistically significant. The experimental data of all groups were processed and organized using Origin 2024.

2.2.2. Transcriptome Sequencing

Based on plate culture assay results, *L. edodes* mycelia were treated with 40 μg/mL Fe^{2+}, 1200 μg/mL K^{+}, and 50 μg/mL Mn^{2+}, with a control group (CK) lacking additional metal-ion supplementation set up simultaneously. Total RNA was extracted from the samples using the Total RNA Extractor (Trizol) kit at Shanghai Sangon Biotech Co., Ltd. Three biological replicates were performed for each treatment, and the DNBSEQ-T7 platform (MGI, Shenzhen, China) was used for transcriptome sequencing (RNA-seq). The raw sequence data were subjected to FastQC for visual quality assessment, and clean reads were obtained using fastp[25]. The clean sequence reads were aligned with the reference genome using HISAT2[26], and RSeQC analyzed the alignment[27].

2.2.3. Gene Expression Level Analysis

The transcriptome assembly was performed using StringTie on the basis of alignment results[28], followed by a known gene model comparison with GffCompare to identify novel transcriptional regions. Gene expression levels were quantified using FeatureCounts with the known gene model[29], and TPM (Transcripts Per Million) was used to estimate relative gene expression[30].

2.2.4. Differential Gene Expression and Enrichment Analyses

Differential gene expression analysis was performed through DESeq2[31], topGO for Gene Ontology (GO) functional enrichment analysis (GO database: http://www.geneontology.org), and clusterProfiler for Kyoto Encyclopedia of Genes and Genomes (KEGG) pathway enrichment analysis (KEGG database: http://www.kegg.jp). The clusterProfiler and enrichplot packages in R were used to perform Gene Set Enrichment Analysis (GSEA).

2.2.5. Quantitative Real-Time PCR (qRT-PCR) Validation

Three common differentially expressed genes (DEGs) were selected for qRT-PCR validation. The primers used are presented in Table 1. The β-tubulin 2 gene (C8R40DRAFT_1124140) was taken as the reference gene for expression normalization. Three biological replicates were set for each treatment, with three technical replicates for each sample.

Table 1. Primers for qRT-PCR.

Gene	Putative function	Primer sequence (5′→3′)	
		Forward	Reverse
C8R40DRAFT_1124140	β-tubulin 2	GTTCGCGGTCCCTTAGCTT	GTAATCACCCACATCCTTTTGC
C8R40DRAFT_1243050	pyridoxal phosphate-dependent transferase	CCCATTGACCACTGCCATC	CCAGCCCACATCGACTCC
C8R40DRAFT_1049432	fungal peroxidase	GCTACGCTGTCGCAAGTCC	CCGTCCATGAATCCGAAATC
C8R40DRAFT_1053020	uracil phosphoribosyltrans	CTCTTGTGCTCGAGACAGGCT	TCAGTGGCATCTTTGACCGTT

 doi:10.20944/preprints202604.1406.v1

	ferase-domain-containing protein

3. Results

3.1. Plate Culture Assay

As shown in Figure 1A, Fe^{2+} at a concentration of 10 μg/mL had no significant effect on the mycelial growth of *L. edodes*, whereas at concentrations exceeding 20 μg/mL, it revealed a significant inhibitory effect, with the inhibitory efficacy intensifying as the concentration increased. At 40 μg/mL, the mycelial growth radius on day 7 of incubation decreased by 33.43% compared with the control group.

As shown in Figure 1B, the mycelial growth of *L. edodes* is significantly promoted by Mn^{2+} at concentrations of 50 μg/mL and 100 μg/mL, with the optimal effect observed at 50 μg/mL. In contrast to the control group, the mycelial growth radius reached 23.55 ± 0.37 mm on day 7 with an increase of 10.77%. An obvious inhibitory effect was observed when the concentration exceeded 150 μg/mL, and consequently, the inhibition became more prominent.

As shown in Figure 1C, the mycelial growth of *L. edodes* is significantly promoted by K^+, with the most vigorous mycelial growth detected at a concentration of 1200 μg/mL. The mycelial growth radius was 25.99 ± 0.68 mm on day 7, an increase of 21.22% relative to the control group. Further increase in concentration deteriorated the promoting effect, yet K^+ still exhibited a promotional effect even at 2000 μg/mL.

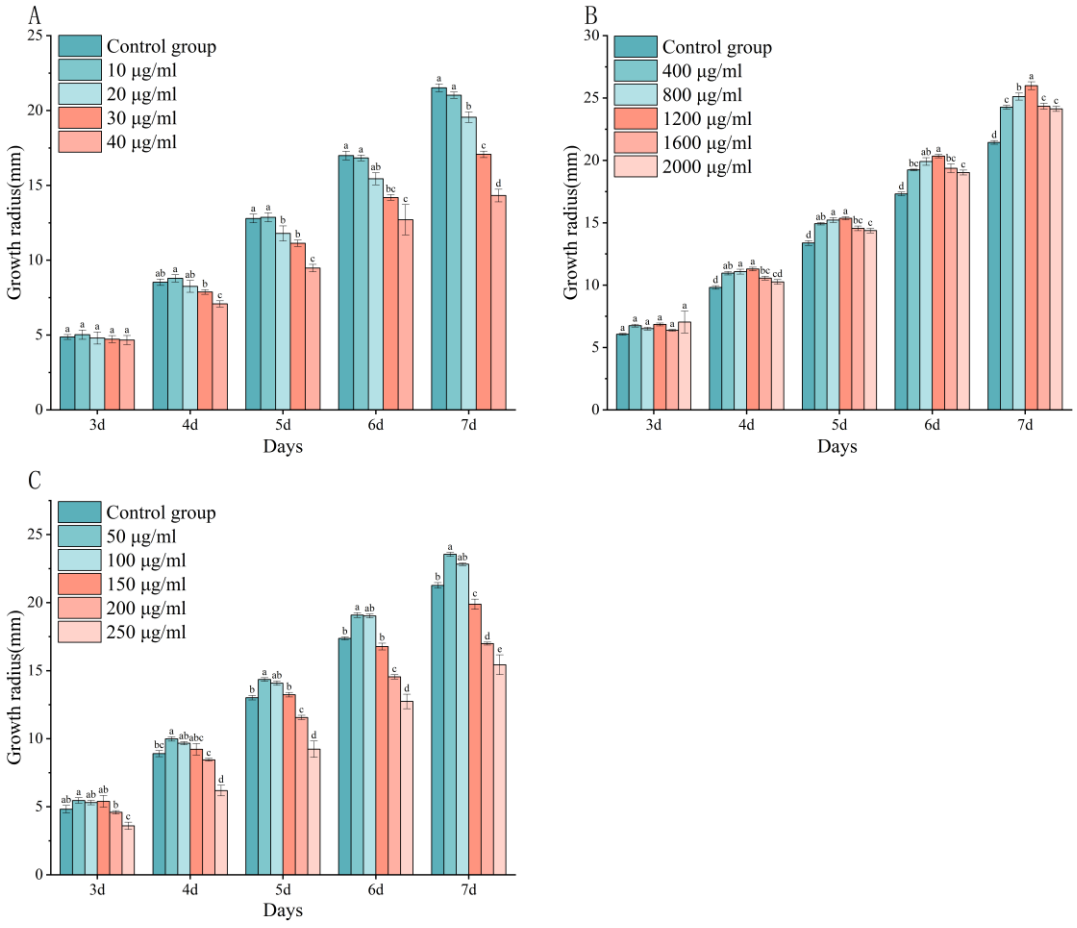

Figure 1. Bar chart of mycelial growth radius in different treatment groups. (**A**) Fe^{2+} treatment, (**B**) K^+ treatment, (**C**) Mn^{2+} treatment.

 doi:10.20944/preprints202604.1406.v1

3.2. Transcriptome Analysis

3.2.1. Raw Data and Sequencing Quality Assessment

High-throughput sequencing was performed on 12 samples from four treatment groups (CK, Fe, K, Mn), with Q30 values exceeding 95% for all samples. Each sample yielded an average of 1.3 gigabytes of high-quality sequencing data, with Q30 values all above 98%, stable GC content, and high data quality after quality control of the raw data (Table 2). The alignment efficiency of each sample's read length to the reference genome ranged from 80.93%–84.56%. Uniquely mapped to the reference gene sequences included 79.61%–83.25% of the filtered read length, and 1.11%–1.40% were multi-mapped. These results indicated high-quality transcriptome sequencing data, suitable for downstream analyses.

Table 2. Transcriptome sequencing data.

Sample No.	Raw Reads Count	Raw Bases Count	Clean Reads Count	Clean Bases Count	Q30 Bases Ratio(%)	GC content (%)
CK1	99,954,944	14,993,241,600	94,629,298	13,353,955,541	98.91%	48.79%
CK2	122,742,912	18,411,436,800	88,535,680	12,526,057,802	98.71%	48.69%
CK3	100,000,000	15,000,000,000	116,115,398	16,309,407,246	98.87%	48.48%
Fe1	100,000,000	15,000,000,000	93,037,640	13,060,762,548	98.81%	48.84%
Fe2	100,000,000	15,000,000,000	93,798,908	13,141,156,027	98.83%	48.96%
Fe3	100,000,000	15,000,000,000	94,475,116	13,426,499,466	98.79%	48.85%
K1	100,000,000	15,000,000,000	93,847,592	13,266,192,738	98.86%	48.78%
K2	100,000,000	15,000,000,000	94,226,408	13,230,205,439	98.86%	48.94%
K3	100,000,000	15,000,000,000	94,796,364	13,405,157,343	98.87%	48.91%
Mn1	94,438,218	14,165,732,700	94,218,924	13,258,424,776	98.88%	48.74%
Mn2	100,000,000	15,000,000,000	95,295,406	13,439,817,749	98.77%	48.67%
Mn3	101,680,028	15,252,004,200	94,191,118	13,167,217,379	98.82%	48.90%

3.2.2. Expression Level Analysis

TPM values from the sequencing data for each sample were calculated, and density curves and violin plots of gene expression levels were subsequently generated (Figure 2), providing valuable insights into the distribution characteristics of gene expression levels in each sample and enabling direct comparison of overall gene expression levels across distinct samples. A uniform distribution of gene expression levels across all *L. edodes* samples was revealed by the density curves, with minor differences among samples, and the TPM values of most genes were concentrated in the range of 1–100 in each sample. A wide distribution range of TPM values was observed in the violin plots across all samples, and the $\log_2$(TPM) values of the majority of genes in each sample were concentrated between 0 and 10.

 doi:10.20944/preprints202604.1406.v1

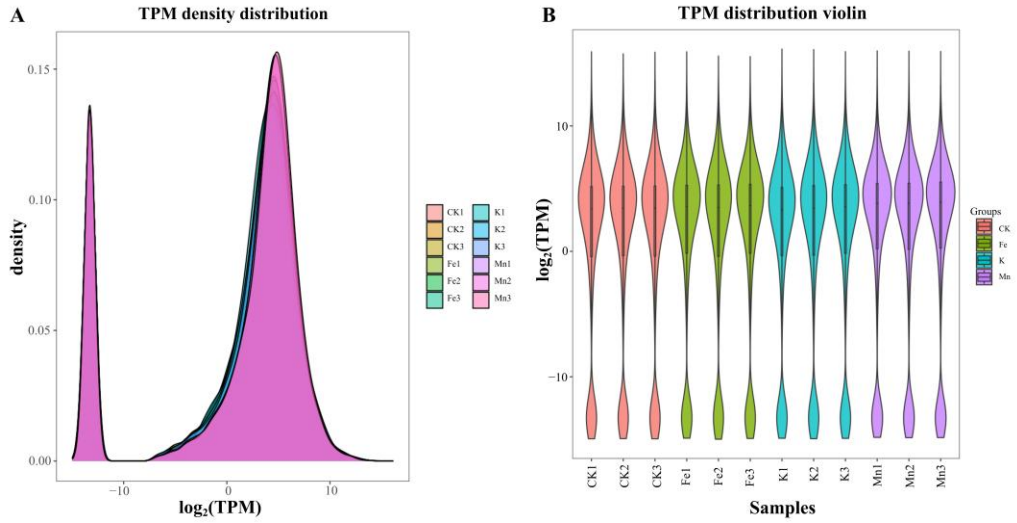

Figure 2. Density curve (**A**) and violin plot (**B**) of gene expression levels.

The PCA plot of *L. edodes* across all treatment groups (Figure 3) showed a high degree of similarity among biological replicates, indicating their suitability for subsequent analyses by the close clustering of the treatments within the replicates. Samples from different treatments were widely dispersed, indicating significant differences among the treatment groups.

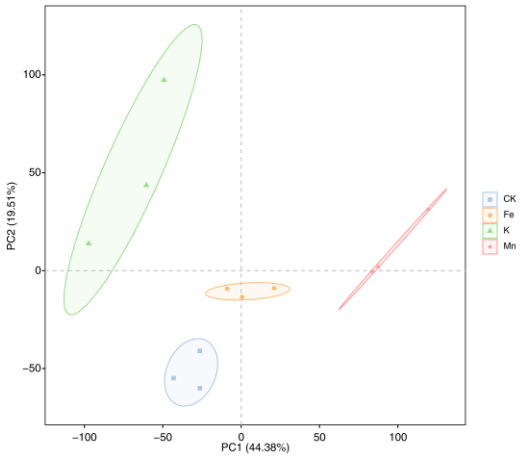

Figure 3. PCA principal component analysis plot.

3.2.3. Differential Gene Expression Analysis

The statistics of the number of differentially expressed genes in *L. edodes* samples are presented in Table 3. Volcano plots visually displayed the up- and down-regulation of significant genes between the two sample groups (Figure 4). The gene expression was weakly affected by the Fe^{2+} treatment group; significant differential expression and a moderate magnitude of change were displayed by only a small number of genes. The K^{+} treatment group exhibited the strongest regulatory intensity over gene expression, significantly driving the high-magnitude expression of many genes. The Mn^{2+} treatment group had many genes showing extreme up- or down-regulation, indicating a more complex regulatory pattern.

 doi:10.20944/preprints202604.1406.v1

Table 3. Number of DEGs in each treatment group.

Treatment	Number of DEGs	Up-regulated genes	Down-regulated genes
Fe^{2+}	226	101	125
K^{+}	858	536	322
Mn^{2+}	696	289	407

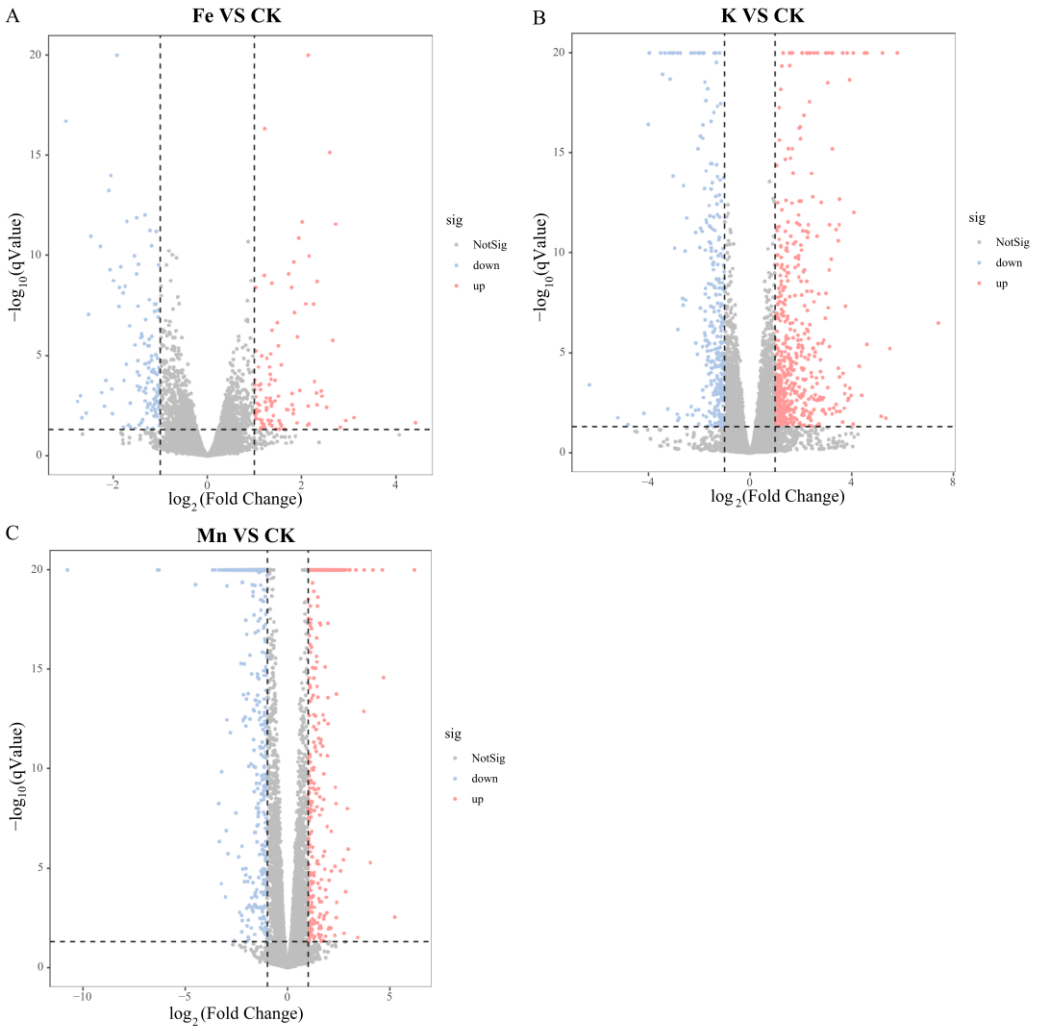

Figure 4. Volcano plot of gene differences in comparison groups. (**A**) Fe^{2+} treatment; (**B**) K^{+} treatment; (**C**) Mn^{2+} treatment. Limits defined by qValue ≤ 0.05 and $|\log_2(\text{Fold Change})| \geq 1$. Each dot in the plot represents a single gene, with red dots indicating up-regulated genes, blue dots indicating down-regulated genes, and gray area represents insignificant genes.

3.2.4. GO Functional Enrichment Analysis

Gene Ontology (GO) functional enrichment analysis annotated the differentially expressed genes (DEGs) into three categories: molecular function (MF), cellular component (CC), and biological process (BP)[24]. In the Fe^{2+}, K^{+}, and Mn^{2+} treatment groups, 17, 106, and 76 differentially expressed genes (DEGs) were annotated in the GO database, assigned to 477, 1933, and 1797 GO terms, respectively, with 3, 19, and 1 terms presenting substantial enrichment (Figure 5A, B, and C).

The differentially expressed genes were significantly enriched in biological processes under Fe^{2+} treatment, including responses to misfolded protein and cellular responses to misfolded protein, as well as the molecular function of misfolded protein binding, with significantly down-regulated genes. Gene Set Enrichment Analysis (GSEA, Figure 7) revealed significantly upregulated ribosome

 doi:10.20944/preprints202604.1406.v1

biogenesis and RNA metabolism-associated functions, including ribonucleoprotein complex biogenesis, RNA processing, rRNA processing, rRNA metabolic process, ribosome biogenesis, preribosome, large subunit precursor, and small-subunit processome.

The differentially expressed genes were significantly enriched in biological processes, including alkaloid biosynthetic process, alkaloid metabolic process, cellular detoxification, secondary metabolite biosynthetic process, secondary metabolic process, and response to toxic substance under K^+ treatment, with significantly up-regulated related genes. These genes were also significantly enriched in molecular functions, including oxidoreductase activity and catalytic activity, with the majority of related genes being up-regulated. GSEA results revealed strong enrichment and overall up-regulation of mitochondrial-related functions, including the significantly enriched mitochondrial protein-containing complex, along with the inner mitochondrial membrane protein complex, mitochondrial transmembrane transport, mitochondrial inner membrane, mitochondrial envelope, mitochondrial transport, and mitochondrial translation.

The differentially expressed genes were significantly enriched in response to toxic substances under Mn^{2+} treatment and primarily concentrated in biological processes, including protein homooligomerization, DNA recombinase assembly, DNA repair complex assembly, detoxification, and protein complex oligomerization. GSEA results revealed significant enrichment and overall down-regulation of purine ribonucleotide metabolic process, carbohydrate derivative metabolic process, and ATP metabolic process, while related functions, including chromosome, nuclear division, DNA recombination, DNA binding, cell cycle, DNA metabolic process, and DNA replication, were significantly enriched and exhibited overall up-regulation.

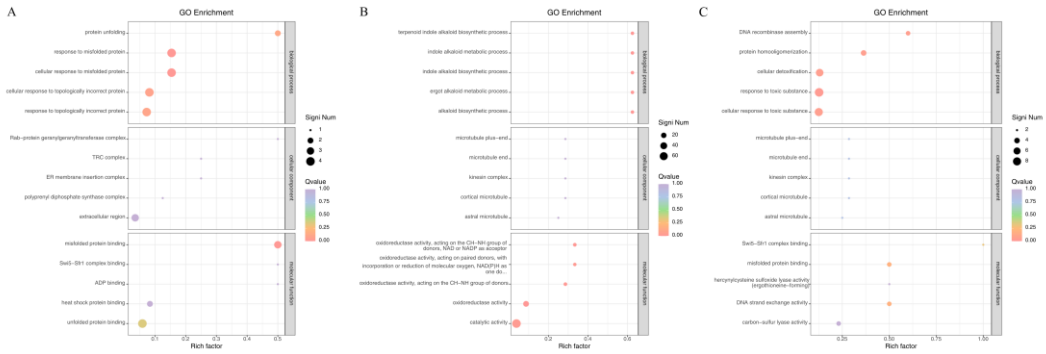

Figure 5. Scatter plot of significantly enriched GO functions of differentially expressed genes. (**A**) Fe^{2+} treatment; (**B**) K^+ treatment; (**C**) Mn^{2+} treatment. The vertical axis represents the functional annotation information, and the horizontal axis denotes the Rich factor corresponding to each function (the number of differentially expressed genes annotated to the function divided by the total number of genes annotated to the function). The magnitude of Qvalue is indicated by the color of the dots, with a smaller Qvalue corresponding to a color closer to red. The size of the dots reflects the number of differentially expressed genes included in each function. After sorting by Qvalue, the top 5 Terms for BP, CC, and MF were respectively selected and plotted in the order of the Rich factor.

3.2.5. KEGG Pathway Enrichment Analysis

The Kyoto Encyclopedia of Genes and Genomes (KEGG) analyses are presented in Figure 6A, B, and C. A total of 22, 134 and 115 differentially expressed genes from the Fe^{2+}, K^+, and Mn^{2+} treatment groups were annotated to 18, 113 and 81 pathways, respectively.

KEGG enrichment analysis of the Fe^{2+} treatment group revealed robust enrichment in the pathways of starch and sucrose metabolism, tyrosine metabolism, styrene degradation, isoquinoline alkaloid biosynthesis, and protein processing in the endoplasmic reticulum, with the corresponding genes significantly down-regulated. In eukaryotic pathways, GSEA indicated significant enrichment and up-regulation of ribosome biogenesis, while cyano amino acid metabolism, tyrosine metabolism, pyruvate metabolism, glycolysis/gluconeogenesis, starch and sucrose metabolism, other glycan

 doi:10.20944/preprints202604.1406.v1

degradation, histidine metabolism, and fatty acid degradation showed overall down-regulation. These pathways contribute to supplying energy and substance metabolism, and deficiencies in ATP, carbon precursors, and other substances required for mycelial growth are directly triggered by their inhibition.

The histidine metabolism pathway was significantly enriched in the K^+ treatment group. Furthermore, the pathways of starch and sucrose metabolism, cyanoamino acid metabolism, glycerolipid metabolism, ascorbate and aldarate metabolism, limonene degradation, glutathione metabolism, steroid biosynthesis, tryptophan metabolism, and methane metabolism were strongly enriched. Significant enrichment and up-regulation of the oxidative phosphorylation and thermogenesis pathways were revealed by GSEA.

The pentose and glucuronate interconversion pathway was significantly enriched under Mn^{2+} treatment. Moreover, the strongly enriched pathways included drug metabolism—cytochrome P450, glutathione metabolism, taurine and hypotaurine metabolism, metabolism of xenobiotics by cytochrome P450, fructose and mannose metabolism, histidine metabolism, ascorbate and aldarate metabolism, and tyrosine metabolism. GSEA indicated significant enrichment and overall up-regulation of the meiosis-yeast and cell cycle pathways, as well as significant enrichment and overall down-regulation of the oxidative phosphorylation and protein processing in endoplasmic reticulum pathways.

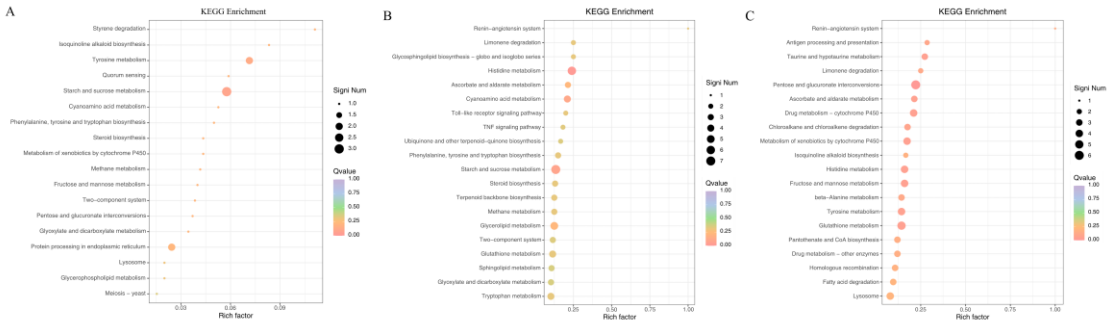

Figure 6. Scatter plot of significantly enriched KEGG functions of differentially expressed genes. (**A**) Fe^{2+} treatment; (**B**) K^+ treatment; (**C**) Mn^{2+} treatment. The vertical axis represents pathway annotation information, and the horizontal axis denotes the corresponding Rich factor (the number of differentially expressed genes annotated to a pathway divided by the total number of genes annotated to that pathway). The magnitude of Qvalue is indicated by the color of the dots, with a smaller Qvalue corresponding to a color closer to red. The size of the dots reflects the number of differentially expressed genes included in each pathway. The pathways with the top significance were selected and plotted in the order of the Rich factor.

 doi:10.20944/preprints202604.1406.v1

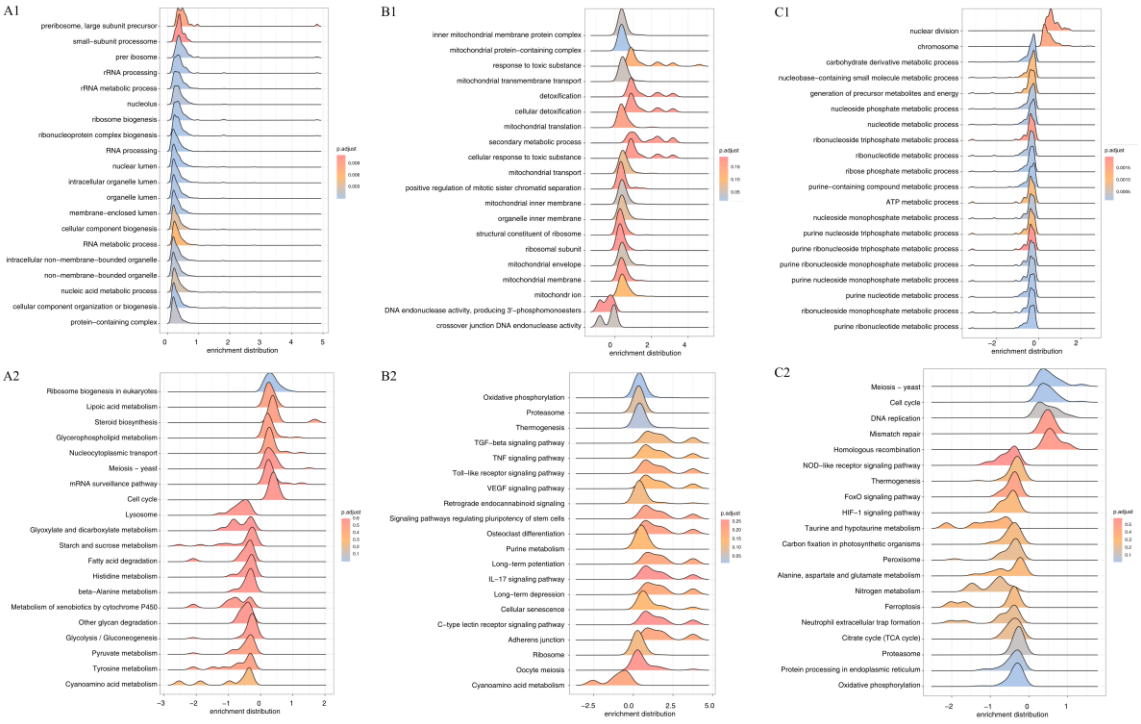

Figure 7. GSEA ridge plot. (**A**) Fe^{2+} treatment, (**B**) K^{+} treatment, (**C**) Mn^{2+} treatment.; (**1**) GO functional enrichment; (**2**) KEGG pathway enrichment. The horizontal axis represents the distribution range of log_2-transformed fold change values of core-enriched genes in the enriched pathways, and the vertical axis denotes the frequency of enriched gene distribution in each pathway. The legend indicates the significance level of GSEA enrichment, with smaller values representing higher significance. The adjusted P-value (p.adjust) was used for analysis, and the top significant functions or pathways were selected and plotted in order of enrichment score.

3.3. Quantitative Real-Time PCR Validation

The expression profiles of the selected differentially expressed genes were generally consistent with the transcriptome sequencing data (Figure 8), ensuring the reliability and accuracy of the transcriptome data and the research results.

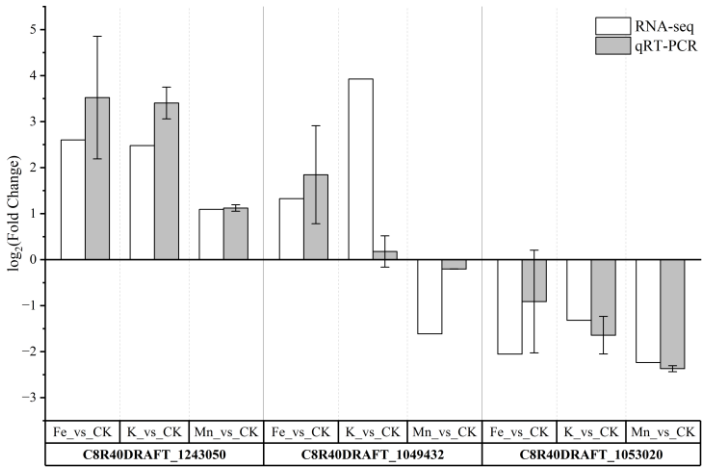

Figure 8. Verification of differential gene expression by qRT-PCR. The qRT-PCR values for each gene are means ± SD of three biological replica.

 doi:10.20944/preprints202604.1406.v1

4. Discussion

In this study, combining plate culture with transcriptomics, we systematically elucidated the regulatory mechanisms of three metal ions (Fe^{2+}, K^+, and Mn^{2+}) on the mycelial growth of *Lentinula edodes* strain 1303. It was confirmed that the effects of metal ions on *L. edodes* mycelial growth are concentration-dependent and element-specific. The phenotypic differences in mycelial growth promotion or inhibition are ultimately caused by different metal ions that regulate distinct gene functions and metabolic pathways.

This study revealed that Fe^{2+} exerted a significant, concentration-dependent inhibitory effect on *L. edodes* mycelial growth at concentrations exceeding 20 μg/mL. The significant inhibitory effect of 50 mg/L Fe^{2+} on *L. edodes* strains U6-11 and U6-12 was demonstrated by Umeo, S. H. *et al.*[6], corroborating the conclusion that *L. edodes* has a weak capacity for biological accumulation and bioavailability of Fe^{2+}[6,7]. The HSP20-like chaperone gene and chaperonin 10-like protein gene were significantly down-regulated under Fe^{2+} treatment. Cellular homeostasis is maintained by oligomeric mitochondrial matrix chaperone proteins[32], heat shock proteins (HSPs), under various environmental stress conditions, with core functions that include ensuring proper protein folding during biosynthesis and preventing misfolding[33,34]. A protein quality-control network could be formed by HSP20 interacting with chaperones, thus maintaining the stability of enzyme function under stress[32]. The correct folding of partially folded or misfolded proteins could be promoted by molecular chaperonins (CPN) under stress; chaperonin 60 (CPN60) and co-chaperonin 10 (CPN10) facilitate the correct folding of nascent proteins by acting synergistically in an ATP-dependent manner[35]. Recycling of misfolded proteins is facilitated by the nucleotide exchange factor Fes1-domain-containing protein gene, which was also significantly down-regulated[36]. Several metal ion transport-related genes, including the IucC family-domain-containing protein gene and the MFS general substrate transporter gene, were significantly down-regulated. Furthermore, a large number of genes related to carbohydrate and amino acid metabolism were significantly down-regulated, including glycoside hydrolase family 5 protein, β-D-xylosidase/β-D-glucosidase, and pyridoxal phosphate-dependent transferase genes. The mycelial growth is inhibited due to a decline in metabolic function.

Within the K^+ concentration gradient used in this study, K^+ consistently promoted *L. edodes* mycelial growth, with the most pronounced effect at 1200 μg/mL, making it the most effective promoter among the three core metal ions. This aligns with the function of K^+ as one of the most important minerals in organisms, driving basic physiological processes, including regulating cellular osmotic pressure and activating enzymes[37,38]. This study revealed significant upregulation of numerous energy metabolism-related genes, including the NAD-P-binding protein gene and the FAD/NAD-binding domain-containing protein gene, providing the adenosine triphosphate (ATP) and reducing power necessary for mycelial growth[22,39]. Further, significant upregulation was observed in carbohydrate metabolism-related genes, including glucoamylase, short-chain dehydrogenase/reductase, and α-amylase genes, which provide sufficient carbon sources for mycelial growth. The HSP20-like chaperone gene and GroES-like protein gene[40] were significantly up-regulated and functional, in sharp contrast to Fe^{2+} treatment. This study is consistent with the previous findings that overexpression of HSP20 can promote mycelial growth in *L. edodes*[41]. A significant upregulation was observed in the glutamate-cysteine ligase catalytic subunit (GCLC) gene, a subunit of glutamate-cysteine ligase (GCL), and the rate-limiting enzyme for intracellular glutathione (GSH) synthesis, which can protect cells from oxidative stress-induced damage[21,42]. Consequently, K^+ significantly enhances energy supply, metabolic processes, and detoxification capacity, promoting the mycelial growth of *L. edodes*.

A significant promotional effect of Mn^{2+} was observed on the mycelial growth of *L. edodes* at 50 μg/mL, but the effect shifted to inhibition at concentrations exceeding 150 μg/mL, signifying a typical concentration effect of promotion at low concentrations and inhibition at high concentrations. Research indicated that the mycelial growth of degenerated *Volvariella volvacea* is promoted by the optimal concentration of 50 mg/L manganese sulfate[13]. Transcriptomic results revealed a

 doi:10.20944/preprints202604.1406.v1

significant up-regulation in the Rad51-domain-containing protein gene and the recombination protein Rad52 gene. For the homologous recombination (HR) in eukaryotes, RAD51 acts as a core recombinase and a key catalytic protein for completing DNA double-strand break repair, while RAD52 loads RAD51, and both of them mutually facilitate homologous recombination repair[43]. Simultaneously, a considerable upregulation was observed in the SNF2 family N-terminal domain-containing protein gene and the helicase C-terminal domain-containing protein gene, both of which play critical roles in transcriptional regulation, DNA replication, and DNA damage repair[44,45]. Furthermore, the glutathione S-transferase III and glutathione-disulfide reductase genes were significantly up-regulated and annotated for multiple detoxification-related functions and pathways. These genes constitute the glutathione antioxidant system and participate in detoxification and secondary metabolic processes[46,47]. Combining the results of gene expression and gene enrichment analyses, it is speculated that Mn^{2+} mainly enhances the proliferative capacity of mycelial cells, promoting mycelial growth. However, further investigation is still required to elucidate the down-regulation of functions and pathways related to energy supply and substance metabolism.

A significant up-regulation was observed in the serine protease inhibitor genes across all three metal-ion treatments. The protease activity is partially or completely inhibited by serine protease inhibitors, which form complexes with their corresponding proteases, maintaining cellular homeostasis and responding to environmental stimuli[48]. This proposes that *L. edodes* can produce functional serine protease inhibitors by regulating metal ions. Many cytochrome P450-related genes showed significant changes across the three treatments and were involved in detoxification processes. Cytochromes P450 (CYP) belong to heme-containing monooxygenases, and fungi possess a more diverse family of cytochromes P450 than plants, animals, or bacteria. In fungi, a wide range of cytochrome P450 enzymes is involved not only in xenobiotic metabolism and virulence regulation but also in the production of numerous secondary metabolites[49].

5. Conclusions

This study investigated the effects of three metal ions on the mycelial growth of *Lentinula edodes*. Among them, the optimal promoting effects were observed by 1200 μg/mL K^+ and 50 μg/mL Mn^{2+}, while mycelial growth was significantly inhibited by Fe^{2+} at concentrations beyond 20 μg/mL. Transcriptomic results revealed Fe^2 primarily induces abnormal protein folding and represses metabolic and substance synthesis pathways, obstructing mycelial growth. The K^+ activates secondary metabolism and detoxification functions, promotes mitochondrial processes and the oxidative phosphorylation pathway, and enhances energy supply, metabolic levels, and detoxification capacity, promoting mycelial growth. Mn^{2+} enhances responses to toxic substances, cell cycle progression, DNA replication and repair, and other related functions, accelerating the division and proliferation of mycelial cells and promoting *L. edodes* mycelial growth. Briefly, this study elucidates the regulatory effects and mechanisms of different metal ions on L. edodes mycelial growth at phenotypic and molecular levels. It provides a scientific basis for optimizing mineral nutrition and developing high-yield cultivation techniques for *L. edodes*, and offers a methodological reference for related studies in other edible fungi. Future studies should focus on the key functional genes and regulatory networks underlying metal ion regulation to provide an experimental basis for high-quality and efficient cultivation of *L. edodes*.

Author Contributions: Conceptualization, H.W. and S.Z.; methodology, H.W., S.Z. and R.H.; investigation, S.Z., R.H. and X.P.; resources, H.W. and S.Z.; data curation and visualization, S.Z. and R.H.; writing—original draft preparation, S.Z. and X.P.; writing—review and editing, H.W. and S.Z.; supervision and project administration, H.W.; funding acquisition, H.W. All authors have read and agreed to the published version of the manuscript.

Funding: This research received no external funding.

Institutional Review Board Statement: Not applicable.

 doi:10.20944/preprints202604.1406.v1

Informed Consent Statement: Not applicable.

Data Availability Statement: The original contributions presented in this study are included in the article. Further inquiries can be directed to the corresponding authors

Acknowledgments: The authors gratefully acknowledge Shanghai Sangon Biotech Co., Ltd. for their support in transcriptome sequencing, and Meiyi Editing for their professional language polishing service.

Conflicts of Interest: The authors declare no conflicts of interest.

Abbreviations

The following abbreviations are used in this manuscript:

CYP	cytochrome P450
DEG	differentially expressed gene
GCLC	glutamate-cysteine ligase catalytic subunit
GCL	glutamate-cysteine ligase
GSH	glutathione
GSEA	gene set enrichment analysis
GO	gene ontology
HSP	heat shock protein
KEGG	Kyoto Encyclopedia of Genes and Genomes
MF	molecular function
CC	cellular component
BP	biological process
PCA	principal component analysis
qRT-PCR	quantitative real-time polymerase chain reaction
RNA-seq	RNA sequencing
TPM	transcripts per million

References

1. Shi, D.; Yin, C.; Feng, X.; Zhou, R.; Fan, X.; Qiao, Y.; Yao, F.; Huang, W.; Liu, Y.; Gao, H.; Cheng, W., Effect of Ultrasound and Cellulase Pre-treatment on the Water Distribution, Physical Properties, and Nutritional Components of Lentinula edodes Chips. *Food and Bioprocess Technology* **2020,** 13, 625-636. http://doi.org/10.1007/s11947-020-02422-z.
2. Adil, B.; Xiang, Q. J.; He, M. L.; Wu, Y. T.; Asghar, M. A.; Arshad, M.; Qin, P.; Gu, Y. F.; Yu, X. M.; Zhao, K.; Zhang, X. P.; Ma, M. G.; Chen, Q.; Chen, X. Q.; Yan, Y. H., Effect of sodium and calcium on polysaccharide production and the activities of enzymes involved in the polysaccharide synthesis of Lentinus edodes. *Amb Express* **2020,** 10, 47. http://doi.org/10.1186/s13568-020-00985-w.
3. Galgowska, M.; Pietrzak-Fiecko, R., Mineral Composition of Three Popular Wild Mushrooms from Poland. *Molecules* **2020,** 25, 3588. http://doi.org/10.3390/molecules25163588.
4. Gao, J.; Li, X.; Jia, S.; Zeng, H.; Zheng, B., Structural characterization and antioxidant activity of a glycoprotein isolated from shiitake mushrooms. *Food Bioscience* **2023,** 53, 102608. http://doi.org/10.1016/j.fbio.2023.102608.
5. Zhang, J.; Rida, K.; Wen, J.; Yu, X.; Gu, Y.; He, M.; Chen, Q.; Xiang, Q., Screening of Lentinula edodes Strains for High Polysaccharide Production and In Vitro Antioxidant Activities. *J Fungi (Basel)* **2025,** 11, 347. http://doi.org/10.3390/jof11050347.
6. Umeo, S. H.; Faria, M. G. I.; Dragunski, D. C.; Valle, J. S. D.; Colauto, N. B.; Linde, G. A., Iron Or Zinc Bioaccumulated In Mycelial Biomass Of Edible Basidiomycetes. *An Acad Bras Cienc* **2020,** 92 (suppl 2), e20191350. http://doi.org/10.1590/0001-3765202020191350.
7. Scheid, S. S.; Faria, M. G. I.; Velasquez, L. G.; do Valle, J. S.; Goncalves, A. C., Jr.; Dragunski, D. C.; Colauto, N. B.; Linde, G. A., Iron biofortification and availability in the mycelial biomass of edible and medicinal basidiomycetes cultivated in sugarcane molasses. *Sci Rep* **2020,** 10, 12875. http://doi.org/10.1038/s41598-020-69699-0.

 doi:10.20944/preprints202604.1406.v1

8. Meniqueti, A. B.; Ruiz, S. P.; Faria, M. G. I.; do Valle, J. S.; Gonçalves, A. C., Jr.; Dragunski, D. C.; Colauto, N. B.; Linde, G. A., Iron-enriched mycelia of edible and medicinal basidiomycetes. *Environ. Technol.* **2022,** 43, 1248-1254. http://doi.org/10.1080/09593330.2020.1824023.
9. Ogidi, C. O.; Oyebode, K. O., Assessment of nutrient contents and bio-functional activities of edible fungus bio-fortified with copper, lithium and zinc. *World J Microbiol Biotechnol* **2022,** 39, 56. http://doi.org/10.1007/s11274-022-03500-4.
10. Oyetayo, V. O.; Ogidi, C. O.; Bayode, S. O.; Enikanselu, F. F., Evaluation of biological efficiency, nutrient contents and antioxidant activity of Pleurotus pulmonarius enriched with Zinc and Iron. *Indian Phytopathology* **2021,** 74, 901-910. http://doi.org/10.1007/s42360-021-00410-7.
11. Naeem, A.; Aslam, M.; Saifullah; Mühling, K. H., Lithium: Perspectives of nutritional beneficence, dietary intake, biogeochemistry, and biofortification of vegetables and mushrooms. *Sci. Total Environ.* **2021,** 798, 149249. http://doi.org/10.1016/j.scitotenv.2021.149249.
12. Li, H.; Dai, J.; Shi, Y.; Zhu, X.; Jia, L.; Yang, Z., Molecular Regulatory Mechanism of the Iron-Ion-Promoted Asexual Sporulation of Antrodia cinnamomea in Submerged Fermentation Revealed by Comparative Transcriptomics. *J Fungi (Basel)* **2023,** 9, 235. http://doi.org/10.3390/jof9020235.
13. Wang, Q.; Wang, W.; Wang, Y.; Yun, J.; Zhang, Y.; Zhao, F., Exogenous MnSO(4) Improves Productivity of Degenerated Volvariella volvacea by Regulating Antioxidant Activity. *J Fungi (Basel)* **2024,** 10, 825. http://doi.org/10.3390/jof10120825.
14. Zhang, B.; Zhou, J.; Li, Q.; Gan, B. C.; Peng, W. H.; Zhang, X. P.; Tan, W.; Jiang, L.; Li, X. L., Manganese affects the growth and metabolism of Ganoderma lucidum based on LC-MS analysis. *PeerJ* **2019,** 7, e6846. http://doi.org/10.7717/peerj.6846.
15. Rodriguez Estrada, A. E.; Royse, D. J., Yield, size and bacterial blotch resistance of Pleurotus eryngii grown on cottonseed hulls/oak sawdust supplemented with manganese, copper and whole ground soybean. *Bioresour Technol* **2007,** 98, 1898-1906. http://doi.org/10.1016/j.biortech.2006.07.027.
16. Zieba, P.; Sekara, A.; Bernas, E.; Krakowska, A.; Sulkowska-Ziaja, K.; Kunicki, E.; Suchanek, M.; Muszynska, B., Supplementation with Magnesium Salts-A Strategy to Increase Nutraceutical Value of Pleurotus djamor Fruiting Bodies. *Molecules* **2021,** 26, 3273. http://doi.org/10.3390/molecules26113273.
17. Wlodarczyk, A.; Krakowska, A.; Sulkowska-Ziaja, K.; Suchanek, M.; Zieba, P.; Opoka, W.; Muszynska, B., Pleurotus spp. Mycelia Enriched in Magnesium and Zinc Salts as a Potential Functional Food. *Molecules* **2020,** 26, 162. http://doi.org/10.3390/molecules26010162.
18. Li, X.; Luo, L.; Wang, X.; Zhu, M., Further insights into the molecular mechanisms underlying tobacco straw cultivation of Pleurotus ostreatus by comparative transcriptome analyses. *Genomics* **2025,** 117, 110992. http://doi.org/10.1016/j.ygeno.2025.110992.
19. Xie, M.; Wang, F.; Zhou, X.; Zeng, J.; Zhou, Y.; Wei, T.; Chen, B.-X., Multi-omics approaches for advancing edible fungi: from genomics-enabled strain development to metabolomics-guided postharvest preservation. *Food Bioscience* **2025,** 71, 107161. http://doi.org/10.1016/j.fbio.2025.107161.
20. Wang, J.; Cai, W.; Jin, Q.; Fan, L.; Guo, Z.; Feng, W., Improving the Yield and Quality of Morchella spp. Using Agricultural Waste. *J Fungi (Basel)* **2025,** 11, 703. http://doi.org/10.3390/jof11100703.
21. Lu, F.; Sun, X.; Dai, X.; Zhang, P.; Ma, Y.; Xu, Y.; Wang, L.; Zhang, J., Integrated Multi-Omics Analysis to Investigate the Molecular Mechanisms Underlying the Response of Auricularia heimuer to High-Temperature Stress. *J Fungi (Basel)* **2025,** 11, 167. http://doi.org/10.3390/jof11030167.
22. Kim, J. Y.; Kim, D. Y.; Park, Y. J.; Jang, M. J., Transcriptome analysis of the edible mushroom Lentinula edodes in response to blue light. *PLoS One* **2020,** 15, e0230680. http://doi.org/10.1371/journal.pone.0230680.
23. Deshaware, S.; Marathe, S. J.; Bedade, D.; Deska, J.; Shamekh, S., Investigation on mycelial growth requirements of Cantharellus cibarius under laboratory conditions. *Arch Microbiol* **2021,** 203, 1539-1545. http://doi.org/10.1007/s00203-020-02142-0.
24. Shao, K.; Yao, F.; Fang, M.; Lu, L.; Ma, X.; Wang, W.; Meng, J.; Sun, X.; Cui, Y.; Sun, J., Transcriptome-Based Analysis of Mitochondrial Influence on Key Agronomic Traits and Nutritional Components in Auricularia heimuer. *Agronomy* **2025,** 15, 2188. http://doi.org/10.3390/agronomy15092188.
25. Chen, S. F.; Zhou, Y. Q.; Chen, Y. R.; Gu, J., fastp: an ultra-fast all-in-one FASTQ preprocessor. *Bioinformatics* **2018,** 34, 884-890. http://doi.org/10.1093/bioinformatics/bty560.

 doi:10.20944/preprints202604.1406.v1

26. Kim, D.; Paggi, J. M.; Park, C.; Bennett, C.; Salzberg, S. L., Graph-based genome alignment and genotyping with HISAT2 and HISAT-genotype. *Nat Biotechnol* **2019,** 37, 907-915. http://doi.org/10.1038/s41587-019-0201-4.
27. Wang, L.; Wang, S.; Li, W., RSeQC: quality control of RNA-seq experiments. *Bioinformatics* **2012,** 28, 2184-2185. http://doi.org/10.1093/bioinformatics/bts356.
28. Pertea, M.; Pertea, G. M.; Antonescu, C. M.; Chang, T. C.; Mendell, J. T.; Salzberg, S. L., StringTie enables improved reconstruction of a transcriptome from RNA-seq reads. *Nat Biotechnol* **2015,** 33, 290-295. http://doi.org/10.1038/nbt.3122.
29. Liao, Y.; Smyth, G. K.; Shi, W., featureCounts: an efficient general purpose program for assigning sequence reads to genomic features. *Bioinformatics* **2014,** 30, 923-930. http://doi.org/10.1093/bioinformatics/btt656.
30. Zhao, S. R.; Ye, Z.; Stanton, R., Misuse of RPKM or TPM normalization when comparing across samples and sequencing protocols. *Rna* **2020,** 26, 903-909. http://doi.org/10.1261/rna.074922.120.
31. Love, M. I.; Huber, W.; Anders, S., Moderated estimation of fold change and dispersion for RNA-seq data with DESeq2. *Genome Biol.* **2014,** 15, 38. http://doi.org/10.1186/s13059-014-0550-8.
32. Lang, B. J.; Guerrero, M. E.; Prince, T. L.; Okusha, Y.; Bonorino, C.; Calderwood, S. K., The functions and regulation of heat shock proteins; key orchestrators of proteostasis and the heat shock response. *Arch Toxicol* **2021,** 95, 1943-1970. http://doi.org/10.1007/s00204-021-03070-8.
33. Liang, Z.-Q.; Zhao, Y.; Tan, Y.-Z.; Wang, J.; Shao, Y.-L.; Zheng, Q.-W.; Zou, Y.; Lin, J.-F.; Chen, M.-T.; Ye, Z.-W., Functional characterization of the heat shock protein gene hsp78 in regulating carotenoid biosynthesis in the edible-medicinal fungus Cordyceps militaris. *Food Bioscience* **2025,** 74, 107894. http://doi.org/10.1016/j.fbio.2025.107894.
34. Chen, C.; Li, Q.; Wang, Q.; Lu, D.; Zhang, H.; Wang, J.; Fu, R., Transcriptional profiling provides new insights into the role of nitric oxide in enhancing Ganoderma oregonense resistance to heat stress. *Sci Rep* **2017,** 7, 15694. http://doi.org/10.1038/s41598-017-15340-6.
35. Kumari, A.; Sutariya, J. A.; Rathore, A. P.; Rathore, M. S., The novel chaperonin 10 like protein (SbCPN10L) from Salicornia brachiata (Roxb.) augment the heat stress tolerance in transgenic tobacco. *Gene* **2024,** 900, 148139. http://doi.org/10.1016/j.gene.2024.148139.
36. Kumar, S.; Masison, D. C., Hsp70-nucleotide exchange factor (NEF) Fes1 has non-NEF roles in degradation of gluconeogenic enzymes and cell wall integrity. *PLoS Genet* **2019,** 15, e1008219. http://doi.org/10.1371/journal.pgen.1008219.
37. Zhao, W.; Dong, H.; Zhou, Z.; Wang, Y.; Hu, W., Potassium (K) application alleviates the negative effect of drought on cotton fiber strength by sustaining higher sucrose content and carbohydrates conversion rate. *Plant Physiol Biochem* **2020,** 157, 105-113. http://doi.org/10.1016/j.plaphy.2020.10.014.
38. Gao, Z.; Chen, F.; Zheng, J.; Peng, Q.; Chen, D.; Zhang, Y.; Zhou, L.; Liu, K.; Yang, Y.; Yuan, Q., Potassium-Selective Covalent Organic Framework Membranes Enable Dynamic Monitoring of Microbial K(+) Metabolism. *Small* **2025,** 21, e2502541. http://doi.org/10.1002/smll.202502541.
39. Luo, C.; Song, Y.; Meng, L.; Cheng, Y.; Dai, H.; Qiao, Y.; Xie, X., Transcriptomic insights into the molecular mechanism of abietic acid promoting growth and branching in Armillaria gallica. *Front Microbiol* **2025,** 16, 1632512. http://doi.org/10.3389/fmicb.2025.1632512.
40. Wang, W.; Vinocur, B.; Shoseyov, O.; Altman, A., Role of plant heat-shock proteins and molecular chaperones in the abiotic stress response. *Trends Plant Sci* **2004,** 9, 244-252. http://doi.org/10.1016/j.tplants.2004.03.006.
41. Ling, Y. Y.; Ling, Z. L.; Zhao, R. L., Construction of a heat-resistant strain of Lentinus edodes by fungal Hsp20 protein overexpression and genetic transformation. *Front Microbiol* **2022,** 13, 1009885. http://doi.org/10.3389/fmicb.2022.1009885.
42. Wenhong, L.; Yang, J.; Zhao, Y.; Zhang, N.; Zhao, B.; Rongxian, L.; Shiyan, G.; Zuoshun, H., Cadmium treatment induces oxidative damage and apoptosis in vitro skeletal muscle cells. *Toxicology* **2025,** 515, 154139. http://doi.org/10.1016/j.tox.2025.154139.
43. Deveryshetty, J.; Mistry, A.; Pangeni, S.; Ghoneim, M.; Tokmina-Lukaszewska, M.; Gore, S. K.; Liu, J.; Kaushik, V.; Karunakaran, S.; Taddei, A.; Heyer, W. D.; Ha, T.; Bothner, B.; Antony, E., Mechanism of Rad51

 doi:10.20944/preprints202604.1406.v1

filament formation by Rad52 and Rad55-Rad57 in homologous recombination. *Nat Commun* **2025,** 16, 6685. http://doi.org/10.1038/s41467-025-61811-0.

44. Wang, J.; Sun, Z.; Liu, H.; Yue, L.; Wang, F.; Liu, S.; Su, B.; Liu, B.; Kong, F.; Fang, C., Genome-Wide Identification and Characterization of the Soybean Snf2 Gene Family and Expression Response to Rhizobia. *Int J Mol Sci* **2023,** 24, 7250. http://doi.org/10.3390/ijms24087250.
45. Villemain, J.; Rokosky, C., Abstract 1937 Intrinsic disorder in the C-terminal Domain of the Yeast Srs2 helicase Provides Structural Diversity Essential to Implementing Multi-functional Roles in replication, Recombination and Repair. *Journal of Biological Chemistry* **2024,** 300, 107008. http://doi.org/10.1016/j.jbc.2024.107008.
46. Adam, A. M. A.; Refat, M. S.; Mohamed, M. A., Synthesis and spectroscopic characterizations of noble metal complexes (gold, silver, platinum) in the presence of selenium, and their biological applications as antibacterial, antifungal, and anticancer. *Research on Chemical Intermediates* **2013,** 41, 965-1000. http://doi.org/10.1007/s11164-013-1249-2.
47. Averill-Bates, D. A., The antioxidant glutathione. In *Antioxidants*, Litwack, G., Ed. Elsevier Academic Press Inc: San Diego, 2023; Volume. 121, pp 109-141. http://doi.org/10.1016/bs.vh.2022.09.002.
48. Harish, B. S.; Uppuluri, K. B., Microbial serine protease inhibitors and their therapeutic applications. *Int J Biol Macromol* **2018,** 107, 1373-1387. http://doi.org/10.1016/j.ijbiomac.2017.09.115.
49. Shin, J.; Kim, J. E.; Lee, Y. W.; Son, H., Fungal Cytochrome P450s and the P450 Complement (CYPome) of Fusarium graminearum. *Toxins (Basel)* **2018,** 10, 112. http://doi.org/10.3390/toxins10030112.